

Friction on layered media: How deep do phonons reach?

Miru Lee,^{1,*} Niklas Weber,² Cynthia A. Volkert,² and Matthias Krüger^{1,†}

¹*Institute for Theoretical Physics, Georg-August-Universität Göttingen, 37073 Göttingen, Germany*

²*Institute of Materials Physics, Georg-August-Universität Göttingen, 37073 Göttingen, Germany*

(Dated: May 4, 2022)

We theoretically study the frictional damping of a small probe object on a coated planar surface, analyzing the resulting phonon modes via a theory of viscoelasticity. Three different types of excitations are found to contribute to friction in distinct ways: traveling (3D) spherical waves, traveling (2D) surface waves, and evanescent waves. While traveling waves transport energy away from the probe, determined by long range elastic properties (wavelength), evanescent waves transform energy into heat in a near-field range, characterized by the size of the probe. Thus, fundamentally different behaviors are predicted, depending on coating thickness and material properties.

The phenomenon of sliding friction involves a complex process involving (nonlinear) interactions, and in some cases resulting in stick-slip motion [1–6]. The excitations created by sliding are expected to be converted into heat in the surrounding media, and the relevant degrees of freedom have been found to include both electronic [7–11] and phononic ones [9–21].

The role of phonon modes can be isolated by tuning them while (ideally) keeping the surface properties and the contact mechanics unchanged. This has been achieved in various ways, such as by thermally inducing a phase transition in the solid [11, 17] or by changing an external electric field [18].

Studying friction on layers of different thickness is another way of achieving this goal; it is especially insightful as it not only allows material properties to be tailored while limiting changes in the contact surface, it also reveals how deep friction feels into the material. A number of numerical and nanoscale experimental studies have been done on the effect of layers in the contact area [22–30]. However, the results often appear to be contradictory and no unifying trends are apparent. For example, while adding graphene layers between two sliding bodies can substantially reduce friction [29], both increases [22–24] and decreases [25–28] in friction have been observed as the number of graphene layers is increased. Friction has also been observed to decrease with thickness for other layered materials such as molybdenum disulfide and niobium diselenide, as long as they are weakly bonded to the substrate [28]. In contrast, a molecular dynamics simulation has been shown that sliding friction increases and plateaus upon increasing the sample thickness, when the sample is harmonically bonded to a heat bath which absorbs any incoming phonons [30]. The complexity of the observed behavior calls for a theory that systematically addresses the dependence of phononic damping on layer thickness, boundary conditions, and material properties.

In this manuscript, we analyze friction of a nanoscopic object on a 3D planar coated substrate, treating phonon modes via a field theory of viscoelasticity that includes phonon attenuation. We find that friction arises due to

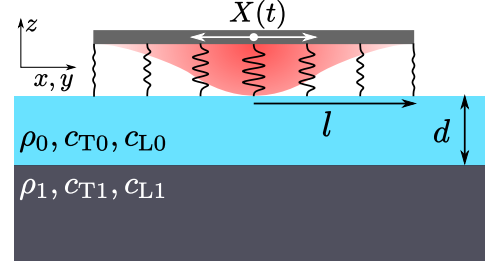


FIG. 1. Investigated system: a probe is coupled to the surface of a coated substrate, and oscillates parallel to it. The coupling interaction carries an interaction radius l . The coating of thickness d and the substrate are characterized by mass density ρ and transverse (c_T) and longitudinal (c_L) speeds of sound, as indicated.

traveling spherical waves, (cylindrical) surface waves, or evanescent waves, each dominating in different regimes of material properties and coating thickness. As a consequence, friction shows a variety of drastically different dependencies on coating thickness ranging from short range to long range behavior, and can increase or decrease with coating thickness. These regimes are determined by the phonon attenuation coefficients and the refractive index.

Consider a probe coupled to an isotropic solid filling the space $z \leq 0$ (see Fig. 1). The probe oscillates parallel to the surface, so that its x coordinate is $X(t) = \text{Re}\{X_0 e^{i\omega t}\}$. The coupling with the surface causes a force acting on the probe, whose x -coordinate is $F(t) = \text{Re}\{F_0 e^{i\omega t}\}$. The damping coefficient Γ is defined as the ratio $\Gamma = \omega^{-1} \text{Im}\{F_0/X_0\}$ [31], which is proportional to the friction force [1–3].

The specific form of coupling is not important for the conclusions of this manuscript, as detailed in the Supplemental Material (SM). We thus use a simple linear one, which will allow us to find analytic expressions,

$$F(t) = n_A \kappa \iint_{-\infty}^{\infty} d^2 \mathbf{r}_{\parallel} (-X(t) + u_x(\mathbf{r}_{\parallel}, t)) e^{-\frac{r_{\parallel}^2}{l^2}}, \quad (1)$$

where $\mathbf{r}_{\parallel} = (x, y, 0)$ marks a position on the surface, and $u_x(\mathbf{r}_{\parallel}, t)$ is the x -component of the phonon field of

the sample at the surface (introduced below). n_A is the particle number per unit area [32], and κ is the coupling strength. Equation (1) contains a Gaussian envelope of width l , introduced to obtain a length scale setting the interaction range or probe size. The force modeled by this equation can thus be understood as harmonic springs connecting the probe to the surface atoms within a radius l (see Fig. 1).

The first term in Eq. (1) is the force in the absence of phonon excitations; it is in phase with $X(t)$ and does not contribute to the damping coefficient Γ . The second term is the force due to excitations of the phonon field \mathbf{u} . This phonon field is treated via a theory of viscoelasticity, i.e., using a Kelvin-Voigt model [33–36],

$$(c_L^2 - c_T^2) \nabla \nabla \cdot \mathbf{u}(\mathbf{r}, \omega) + c_T^2 \nabla^2 \mathbf{u}(\mathbf{r}, \omega) = -\omega^2 \mathbf{u}(\mathbf{r}, \omega). \quad (2)$$

The perturbation of the phonon field due to motion of the probe enters Eq. (2) via a time dependent boundary condition. The resulting solution for u_x appearing in Eq. (1) is thus linear in $X(t)$, and contains a part that is phase shifted with respect to $X(t)$, which gives rise to the damping coefficient Γ . The oscillating probe excites phonons, whereby its motion is damped. The mathematical solution of the laid out problem proceeds via the Green's function of Eq. (2) (see the SM).

Equation (2) is a very general and widely applicable model of phonon dynamics [33–35]. It contains two fundamental modes with longitudinal, $c_L(\omega) = \sqrt{\frac{3K+4\mu-i\omega(3\xi+4\eta)}{3\rho}}$, and transverse, $c_T(\omega) = \sqrt{\frac{\mu-i\omega\eta}{\rho}}$, speeds of sound. Here K and μ (ξ and η) are the bulk and shear elastic (viscous) moduli, respectively, and ρ the mass density. c_T and c_L are complex due to finite viscous moduli, i.e., Eq. (2) contains phonon attenuation. Microscopically, such attenuation may be caused by phonon-phonon, phonon-electron, or phonon-defect scattering. For simplicity of discussion, we assume $c_L(\omega)/c_T(\omega) = \sqrt{3}$, independent of ω , a good approximation for most solids including graphene [14, 37–39]. c_L thus drops out of the discussion in the following.

We start by discussing and recalling the bulk situation, where the coating thickness d in Fig. 1 is formally infinite, a case extensively studied in previous work [14, 15, 36, 40]. In this case, the fundamental solution of Eq. (2) is a spherical wave $\sim e^{i\omega r_{\parallel}/c_{T0}}/r_{\parallel}$ (see the SM), and the damping coefficient reads

$$\Gamma^\infty = \frac{\kappa^2 n_A^2 l^4}{c_{T0}^3 \rho_0} \left(\zeta^{\text{ela}} + \frac{\zeta^{\text{vis}} \eta_0}{c_{T0}^2 \rho_0 l} + \mathcal{O}\left(\frac{1}{Q^2}, \frac{l^2}{\lambda^2}\right) \right), \quad (3)$$

where $\zeta^{\text{ela}} \approx 1.29$ and $\zeta^{\text{vis}} \approx 1.72$ and c_{T0} is the real part of c_{T0} .

In Eq. (3), we have taken the limit of $l \ll \lambda$, i.e., the size of the probe is small compared to the phonon wavelength $\lambda = 2\pi c_{T0}'/\omega$. The oscillation frequency ω of an AFM tip, the so-called washboard frequency of a

probe sliding over an atomistic surface, is typically in the range of 10^2 to 10^5 Hz [9, 12, 13, 17, 18, 26–28]. λ is thus of order of meters and large compared to l , which we take in the range of nanometers. The phonon decay length is given by $Q\lambda$, which defines the quality factor,

$$Q(\omega) = \frac{\mu_0}{\omega \eta_0}. \quad (4)$$

In a typical experimental situation, this number is of order of $Q \sim 10^4$ [41, 42] (see Table I for experimental parameters). The phonon decay length is thus as large as kilometers (recall the ear-on-the-rail-effect), and hence experimentally irrelevant. Despite this, phonon attenuation will be essential for the resulting friction, due to its hidden and underappreciated physical implication.

The two leading terms in Eq. (3) have fundamentally different physical origin. The first corresponds to transport of energy by traveling waves that are excited by the motion of the probe, and it persists in the absence of phonon attenuation. We call it the elastic contribution [36]. The second term in Eq. (3), on the other hand, is proportional to viscosity η_0 , and we called it the viscous contribution, leaving the discussion of its physical origin for below. The relative weight of these two terms is the dimensionless viscosity,

$$\tilde{\eta} = \frac{\eta_0}{c_{T0}' \rho_0 l} = \frac{\lambda}{2\pi Q l}, \quad (5)$$

which depends on material properties and probe size l . The numbers of Table I imply $\tilde{\eta} \sim 10^5$. We thus shall first discuss the case of $\tilde{\eta} \gg 1$, where the bulk case of Eq. (3) reduces to (using $c_{T0}' = \sqrt{\mu_0/\rho_0} + \mathcal{O}(Q^{-2})$)

$$\lim_{\tilde{\eta} \gg 1} \Gamma^\infty = \frac{\zeta^{\text{vis}} \kappa^2 n_A^2 l^3 \eta_0}{\mu_0^2}. \quad (6)$$

Turning to finite values of d , we note that the boundary condition at the interface between coating (labeled with the subscript 0) and substrate (subscript 1) is determined by the refractive index $n(\omega) = c_{T0}(\omega)/c_{T1}(\omega)$ and the ratio of mass densities [44]. It is insightful to start with the special case of $n = 0$, which yields a Dirichlet boundary condition (DBC) of $\mathbf{u}(\mathbf{r}_{\parallel}, -d, \omega) = \mathbf{0}$ [34, 44]. This corresponds to the case where the substrate is much stiffer than the coating, and phonons are totally reflected at the interface, with phase shift of π .

l^a	ω^b	ρ^c	μ^c
1 nm	$10^3 \frac{1}{\text{s}}$	$10^{-23} \frac{\text{kg}}{\text{nm}^3}$	$10 \frac{\text{kg}}{\text{nm s}^2}$

^a Refs. [17, 25, 28]. ^b Refs. [17, 18, 26–28]. ^c Ref. [43].

TABLE I. Parameters typical for AFM experiments on solids: radius of contact l , frequency ω , mass density ρ , and shear elastic modulus μ .

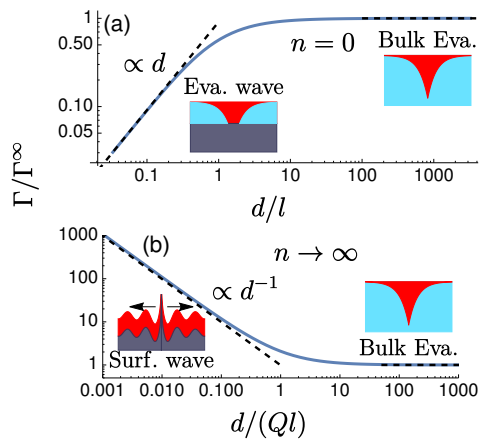


FIG. 2. Damping coefficient Γ for (a) $n = 0$ and (b) $n \rightarrow \infty$ as a function of (scaled) distance d , in the viscous limit $\tilde{\eta} \gg 1$. The solid line shows numerical evaluation, dashed lines give the asymptotes of Eqs. (6), (7) and (8), respectively. Sketches give the fundamental wave solutions in the corresponding regimes.

Figure 2 (a) shows Γ as a function of d for $n = 0$ and $\tilde{\eta} \gg 1$, growing linearly in d for small d , and saturating to the bulk value of Eq. (6) for large d , with a cross-over length scale around $d \approx l$. Indeed, we find that, for small d , the leading order of Γ is linear in d ,

$$\Gamma = \frac{\pi \kappa^2 n_A^2 l^2 \eta_0 d}{2\mu_0^2} + \mathcal{O}(d^3) \stackrel{\tilde{\eta} \gg 1}{\approx} \frac{\pi \Gamma^\infty d}{2\zeta_{\text{vis}} l} + \mathcal{O}(d^3) \quad (\text{DBC}). \quad (7)$$

Γ thus *vanishes* as $d \rightarrow 0$. This can be understood from the insight that the thin coating, when placed on a stiff substrate, supports fewer and fewer phonons as $d \rightarrow 0$.

In the second step in Eq. (7), we used Eq. (6) to replace Γ^∞ . This substitution makes apparent the mentioned saturation to Γ^∞ at $d \approx l$. The dependence of Γ on d is thus of *short range* nature, set by probe size l of Eq. (1), i.e., nanometers.

How is this possible despite the phonon attenuation length of kilometers? The motion of the probe excites not only (attenuated) traveling waves, but also *evanescent waves* that decay within a range of l as a function of distance from the material surface (see the SM). In the presence of finite viscous moduli, they contribute to energy absorption, and thus to the damping coefficient Γ . In Fig. 2, this mechanism outweighs the energy transported by traveling waves, which is why Eqs. (6) and (7) carry η_0 as a factor.

The opposite limit of boundary conditions, $n \rightarrow \infty$, corresponds to a freestanding coating or a much more compliant substrate, and the waves obey a Neumann BC (NBC), $\hat{\mathbf{e}}_z \cdot \boldsymbol{\sigma}(\mathbf{r}_\parallel, -d, \omega) = \mathbf{0}$ where $\boldsymbol{\sigma}$ is the Cauchy stress tensor, and $\hat{\mathbf{e}}_z$ the unit vector in the z direction [44]. Phonons are totally reflected, but without phase shift. In this case, the damping coefficient is fundamentally differ-

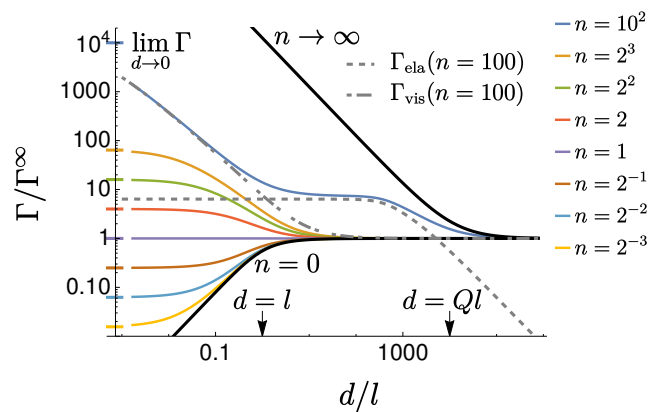


FIG. 3. Damping coefficient Γ for various refractive indices n , using $\tilde{\eta} = 10^5$ and $Q = 10^4$, only considering transverse waves. Marks on the y axis are (analytic) values of $\lim_{d \rightarrow 0} \Gamma$ for the corresponding n . The gray dashed lines are the purely elastic and viscous contributions at $n = 100$.

ent from the case of $n = 0$ as shown in Fig. 2 (b); the friction *diverges* for small d and converges to the bulk value on a scale of $d \approx Ql$. Analytically expanding this case for small d yields

$$\Gamma = \frac{11\pi^2 \kappa^2 n_A^2 l^4}{64\mu_0 |\omega| d} + \mathcal{O}(d) \stackrel{\tilde{\eta} \gg 1}{\approx} \frac{11\pi^2 \Gamma^\infty Ql}{64\zeta_{\text{vis}} d} + \mathcal{O}(d) \quad (\text{NBC}). \quad (8)$$

With a softer substrate, the motion of the probe excites *traveling surface waves*, $\sim e^{i\omega r_\parallel / c_{T0}} / \sqrt{r_\parallel}$, where the coating oscillates like a freestanding 2D sheet. Energy is transported away along the surface, and it is not absorbed, so that Eq. (8) is independent of viscosity η_0 . The divergence with $1/d$ results as the sheet gets more compliant with $d \rightarrow 0$, allowing larger amplitudes of excitations.

The second equality of Eq. (8) implies the mentioned saturation length of $d \approx Ql$. With l on the scale of nanometers, this length is of the order of microns. Thus, for $\tilde{\eta} \gg 1$, neither the wavelength λ (meters) nor the phonon decay length $Q\lambda$ (kilometers) play any role.

The extreme cases of $n = 0$ and $n \rightarrow \infty$ provide a reference for the discussion of an arbitrary refractive index n . For simplicity of discussion, we assume that the quality factors of the coating and substrate are identical, so that the refractive index is real, and use $\rho_0 = \rho_1$ [45]. For finite values of n , we note a numerical challenge in evaluating the longitudinal wave modes, so that we restrict the shown data to transverse waves (see the SM for the proof of validity).

Figure 3 shows Γ as a function of d for various n , at $\tilde{\eta} = 10^5$ and $Q = 10^4$; Γ is monotonic in d , and stays within the bounds of the limiting cases of $n = 0$ and $n \rightarrow \infty$. Importantly, when the coating is vanishingly thin, i.e., $d \rightarrow 0$, Γ approaches the bulk value of the substrate, as shown in the graph on the y -axis. These

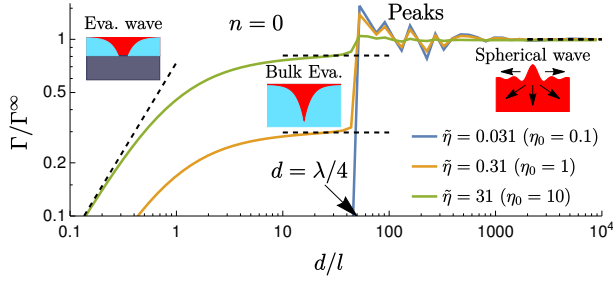


FIG. 4. Damping coefficient Γ as a function of (scaled) distance for $n = 0$, for three values of $\tilde{\eta}$. The black dashed lines represent the asymptotes of Eqs. (3), (6) and (7). For the chosen parameters, the first peak is at $d/l = \lambda/4l \approx 50$.

limiting values are given by Eq. (3) with the material parameters of the substrate [46] [47]. This insight enables us to understand the behavior of Γ seen in Fig. 3 as it varies between the bulk results of the substrate ($d \rightarrow 0$) and of the coating ($d \rightarrow \infty$). These are related by [48],

$$\lim_{d \rightarrow 0} \Gamma = \Gamma^\infty n^3 \frac{\zeta^{\text{ela}} + \zeta^{\text{vis}} \frac{\tilde{\eta}}{n}}{\zeta^{\text{ela}} + \zeta^{\text{vis}} \tilde{\eta}}. \quad (9)$$

Using Eq. (9) allows discussion of Fig. 3. For $\tilde{\eta} \gg 1$ and $\tilde{\eta} \gg n$, Eq. (9) reads $\lim_{d \rightarrow 0} \Gamma \approx n^2 \Gamma^\infty$. Then, for $n < 1$, friction increases with d , while it decreases with d for $n > 1$. The value of $\lim_{d \rightarrow 0} \Gamma$ grows with n^2 , and we see a convergence to the bulk value of the coating on a scale of $d \approx l$.

An exception is the case of $n = 100$ in Fig. 3, where a decay at $d \approx l$ is followed by an intermediate plateau, with a final decay at $d \approx Ql$. Here, the elastic contribution of the substrate (first term in the numerator of Eq. (9)) is larger than the viscous contribution of the coating (second term in the denominator of Eq. (9)). Because the traveling contribution decays more slowly as a function of d , traveling waves dominate for intermediate d as indicated by the gray dashed curves in Fig. 3 at $n = 100$. Comparing the described terms in Eq. (9), such two-step decay is found to appear for $\sqrt[3]{\tilde{\eta}} \lesssim n \lesssim \tilde{\eta}$ (see the SM).

The behavior for $\tilde{\eta} \gg 1$ is summarized in the right part of Fig. 5. For $n < 1$, friction increases with d , and saturates to Γ^∞ at around $d \approx l$. For $1 < n \lesssim \sqrt[3]{\tilde{\eta}}$, it decreases with d , still on a scale of $d \approx l$. In these two cases, friction is dominated by evanescent waves for all d . For $\sqrt[3]{\tilde{\eta}} \lesssim n \lesssim \tilde{\eta}$, we observe a two-step decay (compare $n = 100$ in Fig. 3), dominated by evanescent or traveling waves, as indicated in Fig. 5. For $n \gtrsim \tilde{\eta}$, finally, the small d behavior is dominated by traveling surface waves, crossing over to bulk behavior of evanescent waves at $d \approx Ql$, compare Fig. 2 (b).

What about the case of $\tilde{\eta} \ll 1$ where the limit $d \rightarrow \infty$ is dominated by traveling waves? Despite apparently less experimental relevance, we include this insightful case for

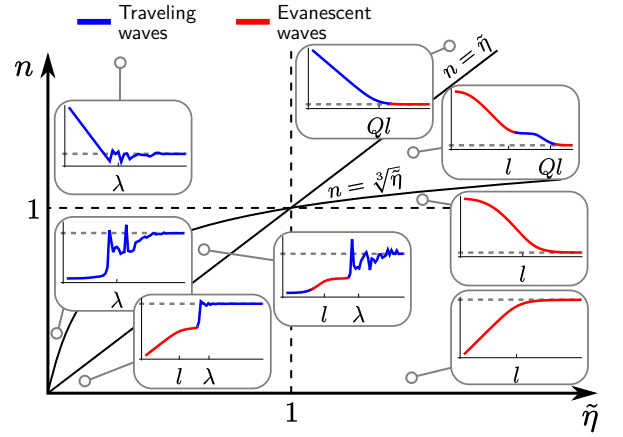


FIG. 5. Friction map. Depending on $\tilde{\eta}$ and n , Γ is dominated by evanescent modes (red lines) and decays to bulk on a scale $d \approx l$, or by traveling waves (blue), which decay on scales of Ql or λ . The lines separating the regimes are deduced from Eq. (9). Gray dashed lines show the limit $d \rightarrow \infty$ of Eq. (3).

completeness. As shown in Fig. 4 for $n = 0$ (see SM for $n \rightarrow \infty$), the behavior for $d \ll \lambda$ is similar to Fig. 2 (a). Notably, for $n = 0$, the coating does not support traveling waves for $d \lesssim \lambda$, and the term in Eq. (7) has no counterpart from traveling waves (SM). For $d \gtrsim \lambda$, traveling waves are excited, yielding a sharp increase of Γ at $d \approx \lambda/4$ followed by peaks; these are due to interference effects, as the reflected wave returns to the probe with a phase shift, contributing constructively or destructively to Γ (see SM). For $d \gg \lambda$, the bulk value of Eq. (3) is approached.

The left-half of Fig. 5 summarizes the behavior for $\tilde{\eta} \ll 1$, which, again, can largely be understood by comparing the terms in Eq. (9). The discussion of Fig. 5 can readily be extended to $\rho_0 \neq \rho_1$ and complex n .

Experiments [28] and MD simulations [25] have reported friction on freely standing graphene flakes, i.e., $n \gg 1$, finding a decrease with increasing number of layers, which is in agreement with the decreasing behavior we describe here. The same holds for mounted graphene layers (or flakes), where the same trend is also observed [25–28]; graphene is much stiffer ($\mu \sim 1$ TPa [39, 49, 50]) than metal substrates ($\mu \sim 10$ GPa [43, 51]), so that the case of $n \gg 1$ applies here as well. We are not aware of friction measurements for compliant coatings on stiffer substrates, a challenge for future work [52] [53].

The framework developed here identifies the main phononic mechanisms for friction between a probe and a coated planar surface. Depending on the coating thickness, refractive index and the viscous moduli, different types of wave modes are excited, each with their own distinct contributions to friction. For systems with high quality factors and short wavelengths, spherical and surface traveling waves are preferentially excited, which contribute to friction by transporting energy away from the

probe. For systems with not too large quality factors and long wavelengths, evanescent waves are the dominant excitation. Rather than transporting, they *dissipate* energy near the vicinity of the probe, contributing to friction. Exceptions exist for thin coatings on stiff substrates, which manifest evanescent waves even for systems with high quality factors, and for thin coatings on compliant substrates, which manifest traveling surface waves even for low quality factors. Thus, depending on the system geometry and properties, friction can show dramatically different behavior that is either governed by near-surface material damping or by long-range wave propagation.

Given the well-known fact that macroscopic friction between two bodies takes place at isolated asperities within the contact area [3, 54], the model presented here can be viewed as describing the contribution from a single asperity. Our findings should therefore give insights into how friction depends on the geometry and material properties at a wide range of dissipative contacts, such as earthquake faults, machining surfaces, and rolling and sliding contacts of all sorts. To date, no obvious overarching trends or patterns in the behavior of general frictional contacts has been found. They show highly varied behavior, with little possibility of prediction. The complex dependence of friction on system geometry and properties presented here for the simple case of a coating on a substrate gives promise that even the complexity of real-life dissipative contacts might be understood.

This work was funded by the Deutsche Forschungsgemeinschaft (DFG, German Research Foundation) - 217133147 via SFB 1073 (Project A01). We thank Richard L.C. Vink for stimulating discussions.

* miru.lee@uni-goettingen.de

† matthias.kruger@uni-goettingen.de

- [1] L. Prandtl, *Zeitschrift für Angewandte Mathematik und Mechanik* **8**, 85 (1928).
- [2] M. H. Müser, *Physical Review B* **84**, 125419 (2011).
- [3] B. N. Persson, *Sliding friction: physical principles and applications* (Springer Science & Business Media, 2013).
- [4] B. N. Persson, O. Albohr, F. Mancosu, V. Peveri, V. Samoilov, and I. M. Sivebæk, *Wear* **254**, 835 (2003).
- [5] E. Gnecco, R. Bennewitz, T. Gyalog, C. Loppacher, M. Bammerlin, E. Meyer, and H.-J. Güntherodt, *Physical Review Letters* **84**, 1172 (2000).
- [6] A. Socoliuc, R. Bennewitz, E. Gnecco, and E. Meyer, *Physical Review Letters* **92**, 134301 (2004).
- [7] I. A. Boldin, A. Kraft, and C. Wunderlich, *Physical Review Letters* **120**, 023201 (2018).
- [8] A. I. Volokitin and B. N. J. Persson, *Physical Review B* **63**, 205404 (2001).
- [9] I. Dorofeyev, H. Fuchs, G. Wenning, and B. Gotsmann, *Physical Review Letters* **83**, 2402 (1999).
- [10] A. I. Volokitin and B. N. J. Persson, *Reviews of Modern Physics* **79**, 1291 (2007).
- [11] M. Kisiel, E. Gnecco, U. Gysin, L. Marot, S. Rast, and E. Meyer, *Nature Materials* **10**, 119 (2011).
- [12] B. Stipe, H. Mamin, T. Stowe, T. Kenny, and D. Rugar, *Physical Review Letters* **87**, 096801 (2001).
- [13] B. Gotsmann and H. Fuchs, *Physical Review Letters* **86**, 2597 (2001).
- [14] B. Persson and R. Ryberg, *Physical Review B* **32**, 3586 (1985).
- [15] A. Volokitin, B. Persson, and H. Ueba, *Physical Review B* **73**, 165423 (2006).
- [16] R. Hu, S. Y. Krylov, and J. W. Frenken, *Tribology Letters* **68**, 1 (2020).
- [17] N. A. Weber, H. Schmidt, T. Sievert, C. Jooss, F. Güthoff, V. Moshneaga, K. Samwer, M. Krüger, and C. A. Volkert, *Advanced Science* **8**, 2003524 (2021).
- [18] H. Schmidt, J.-O. Krisponteit, N. Weber, K. Samwer, and C. A. Volkert, *Physical Review Materials* **4**, 113610 (2020).
- [19] L. Kantorovich, *Physical Review B* **78**, 094304 (2008).
- [20] L. Kantorovich and N. Rompotis, *Physical Review B* **78**, 094305 (2008).
- [21] E. Panizon, G. E. Santoro, E. Tosatti, G. Riva, and N. Manini, *Physical Review B* **97**, 104104 (2018).
- [22] C. Daly and J. Krim, *Physical Review Letters* **76**, 803 (1996).
- [23] S. Kajita, H. Washizu, and T. Ohmori, *Europhysics Letters* **87**, 66002 (2009).
- [24] L. Xu, T.-B. Ma, Y.-Z. Hu, and H. Wang, *Nanotechnology* **22**, 285708 (2011).
- [25] A. Smolyanitsky, J. P. Killgore, and V. K. Tewary, *Physical Review B* **85**, 035412 (2012).
- [26] T. Filleter, J. L. McChesney, A. Bostwick, E. Rotenberg, K. V. Emtsev, T. Seyller, K. Horn, and R. Bennewitz, *Physical Review Letters* **102**, 086102 (2009).
- [27] T. Filleter and R. Bennewitz, *Physical Review B* **81**, 155412 (2010).
- [28] C. Lee, Q. Li, W. Kalb, X.-Z. Liu, H. Berger, R. W. Carpick, and J. Hone, *Science* **328**, 76 (2010).
- [29] D. Berman, A. Erdemir, and A. V. Sumant, *Materials Today* **17**, 31 (2014).
- [30] A. Benassi, A. Vanossi, G. E. Santoro, and E. Tosatti, *Physical Review B* **82**, 081401 (2010).
- [31] H. Risken, *The Fokker-Planck Equation* (Springer, Berlin, 1996).
- [32] H. C. Hamaker, *Physica* **4**, 1058 (1937).
- [33] W. N. Findley, J. S. Lai, and K. Onaran, *Creep and Relaxation of Nonlinear Viscoelastic Materials, with an Introduction to Linear Viscoelasticity* (North-Holland Publishing Company, New York, N.Y., 2013).
- [34] L. Landau, E. Lifshitz, J. Sykes, and W. Reid, *Theory of elasticity: Volume 7 of course of theoretical physics*, Vol. 7 (Elsevier, Oxford, 1986).
- [35] E. Lee, *Quarterly of Applied Mathematics* **13**, 183 (1955).
- [36] M. Lee, R. L. Vink, C. A. Volkert, and M. Krüger, *Physical Review B* **104**, 174309 (2021).
- [37] W. Gornall and B. Stoecheff, *Physical Review B* **4**, 4518 (1971).
- [38] H. Petert, J. Skalyo Jr, H. Grimm, E. Lüscher, and P. Korpiun, *Journal of Physics and Chemistry of Solids* **34**, 255 (1973).
- [39] X. Cong, Q.-Q. Li, X. Zhang, M.-L. Lin, J.-B. Wu, X.-L. Liu, P. Venezuela, and P.-H. Tan, *Carbon* **149**, 19 (2019).
- [40] B. Persson, E. Tosatti, D. Fuhrmann, G. Witte, and C. Wöll, *Physical Review B* **59**, 11777 (1999).

- [41] K. Ono, *Applied Sciences* **10**, 2230 (2020).
- [42] B. N. Persson, *The Journal of Chemical Physics* **115**, 3840 (2001).
- [43] B. A. Auld, *Acoustic fields and waves in solids* (John Wiley & Sons Inc., 1973).
- [44] L. M. Brekhovskikh, *Waves in layered media* (Academic Press, New York, 1980).
- [45] These two assumptions can be relaxed without additional challenge, yielding similar conclusions as the ones presented.
- [46] We assume that the surface coupling (here κ , n_A and l) are the same for coating and for pure substrate.
- [47] In experiments, the limit $d \rightarrow 0$ (thin coating) is expected to be different from $d = 0$ (no coating), because of different surface interactions for substrate and coating.
- [48] Eq. (9) is valid for any value of $\tilde{\eta}$. See the SM for the general case where n is complex and $\rho_0 \neq \rho_1$.
- [49] J.-U. Lee, D. Yoon, and H. Cheong, *Nano letters* **12**, 4444 (2012).
- [50] G. Van Lier, C. Van Alsenoy, V. Van Doren, and P. Geerlings, *Chemical Physics Letters* **326**, 181 (2000).
- [51] J.-H. Zhao, T. Ryan, P. S. Ho, A. J. McKerrow, and W.-Y. Shih, *Journal of Applied Physics* **85**, 6421 (1999).
- [52] The system investigated in Benassi *et al.* [30] uses stochastic boundary conditions, which are not easily mapped on our framework.
- [53] N. Weber, M. Lee, R. L. Vink, V. Moshnyaga, M. Krüger, and C. A. Volkert, In preparation (2022).
- [54] F. P. Bowden, D. Tabor, and G. I. Taylor, *Proceedings of the Royal Society of London. Series A. Mathematical and Physical Sciences* **169**, 391 (1939).

Supplementary Material

Miru Lee,^{1,*} Niklas Weber,² Cynthia A. Volkert,² and Matthias Krüger^{1,†}

¹*Institute for Theoretical Physics, Georg-August-Universität Göttingen, 37073 Göttingen, Germany*

²*Institute of Materials Physics, Georg-August-Universität Göttingen, 37073 Göttingen, Germany*

(Dated: May 4, 2022)

DAMPING COEFFICIENT

The damping coefficient can be calculated from a Green-Kubo relation [1–4],

$$\Gamma = \frac{1}{2k_{\text{B}}T} \int_{-\infty}^{\infty} \frac{d\omega'}{2\pi} \langle F(X, \omega); F(X, \omega') \rangle, \quad (1)$$

where $\langle A; B \rangle = \langle (A - \langle A \rangle)(B - \langle B \rangle) \rangle$ is an ensemble average of the covariance. With the force defined in [Eq. (1)] in the main text, the damping coefficient can be rewritten as

$$\begin{aligned} \Gamma &= \frac{\kappa^2 n_A^2}{2k_{\text{B}}T} \int_{-\infty}^{\infty} d^2 \mathbf{r}_{\parallel} \int_{-\infty}^{\infty} d^2 \mathbf{r}'_{\parallel} \int_{-\infty}^{\infty} \frac{d\omega'}{2\pi} e^{-\frac{r_{\parallel}^2}{t^2}} \langle u_x(\mathbf{r}_{\parallel}, \omega) u_x(\mathbf{r}'_{\parallel}, \omega') \rangle e^{-\frac{r_{\parallel}'^2}{t^2}} \\ &= \frac{\kappa^2 n_A^2}{\omega} \int_{-\infty}^{\infty} d^2 \mathbf{r}_{\parallel} \int_{-\infty}^{\infty} d^2 \mathbf{r}'_{\parallel} e^{-\frac{r_{\parallel}^2}{t^2}} \text{Im}\{G(\mathbf{r}_{\parallel}, \mathbf{r}'_{\parallel}, \omega)\} e^{-\frac{r_{\parallel}'^2}{t^2}} \\ &= \frac{\kappa^2 n_A^2}{\omega} \text{Im} \left\{ \int_{-\infty}^{\infty} d^2 \mathbf{r}_{\parallel} \int_{-\infty}^{\infty} d^2 \mathbf{r}'_{\parallel} e^{-\frac{r_{\parallel}^2}{t^2}} G(\mathbf{r}_{\parallel}, \mathbf{r}'_{\parallel}, \omega) e^{-\frac{r_{\parallel}'^2}{t^2}} \right\} \end{aligned} \quad (2)$$

Note that in the second equality, we make use of the FDT [4–9],

$$\int_{-\infty}^{\infty} \frac{d\omega'}{2\pi} \langle u_x(\mathbf{r}, \omega) u_x(\mathbf{r}', \omega') \rangle = \frac{2k_{\text{B}}T}{\omega} \text{Im}\{G(\mathbf{r}, \mathbf{r}', \omega)\}. \quad (3)$$

It is more convenient to obtain the Green's function in $\mathbf{k}_{\parallel} = (k_x, k_y)$ space, since the Kelvin-Voigt model ([Eq. (2)] in the main text) becomes an ordinary differential equation. Let us change the spatial integral to an integral over \mathbf{k}_{\parallel} space,

$$\begin{aligned} \Gamma &= \frac{\kappa^2 n_A^2}{\omega} \text{Im} \left\{ \int_{-\infty}^{\infty} d^2 \mathbf{r}_{\parallel} \int_{-\infty}^{\infty} d^2 \mathbf{r}'_{\parallel} e^{-\frac{r_{\parallel}^2}{t^2}} G(\mathbf{r}_{\parallel}, \mathbf{r}'_{\parallel}, \omega) e^{-\frac{r_{\parallel}'^2}{t^2}} \right\} \\ &= \frac{\kappa^2 n_A^2}{\omega} \text{Im} \left\{ \int d^2 \mathbf{r}_{\parallel} \int d^2 \mathbf{r}'_{\parallel} \int_{-\infty}^{\infty} \frac{d^2 \mathbf{k}_{\parallel}}{(2\pi)^2} \int_{-\infty}^{\infty} \frac{d^2 \mathbf{k}'_{\parallel}}{(2\pi)^2} e^{-\frac{r_{\parallel}^2}{t^2}} G(\mathbf{k}_{\parallel}, z=0, \mathbf{k}'_{\parallel}, z'=0, \omega) e^{-\frac{r_{\parallel}'^2}{t^2}} e^{i\mathbf{k}_{\parallel} \cdot \mathbf{r}_{\parallel}} e^{i\mathbf{k}'_{\parallel} \cdot \mathbf{r}'_{\parallel}} \right\} \\ &= \frac{\kappa^2 n_A^2 l^4 \pi^2}{\omega} \text{Im} \left\{ \int_{-\infty}^{\infty} \frac{d^2 \mathbf{k}_{\parallel}}{(2\pi)^2} \int_{-\infty}^{\infty} \frac{d^2 \mathbf{k}'_{\parallel}}{(2\pi)^2} e^{-\frac{k_{\parallel}^2 t^2}{4}} G(\mathbf{k}_{\parallel}, 0, \mathbf{k}'_{\parallel}, 0, \omega) e^{-\frac{k_{\parallel}'^2 t^2}{4}} \right\}. \end{aligned} \quad (4)$$

The above expression for the damping coefficient can be further simplified if the homogeneity of the Green's function is assumed, i.e., $G(\mathbf{r} + \mathbf{r}_0, \mathbf{r}' + \mathbf{r}_0, \omega) = G(\mathbf{r}, \mathbf{r}', \omega)$ [10],

$$\begin{aligned} G(\mathbf{k}, \mathbf{k}', \omega) &= \int_{-\infty}^{\infty} d^3 \mathbf{r} \int_{-\infty}^{\infty} d^3 \mathbf{r}' G(\mathbf{r} + \mathbf{r}_0, \mathbf{r}' + \mathbf{r}_0, \omega) e^{-i\mathbf{k} \cdot (\mathbf{r} + \mathbf{r}_0)} e^{-i\mathbf{k}' \cdot (\mathbf{r}' + \mathbf{r}_0)} \\ &= \int_{-\infty}^{\infty} d^3 \mathbf{r} \int_{-\infty}^{\infty} d^3 \mathbf{r}' G(\mathbf{r}, \mathbf{r}', \omega) e^{-i\mathbf{k} \cdot \mathbf{r}} e^{-i\mathbf{k}' \cdot \mathbf{r}'} e^{-i\mathbf{r}_0 \cdot (\mathbf{k} + \mathbf{k}')} \\ &= G(\mathbf{k}, \mathbf{k}', \omega) e^{-i\mathbf{r}_0 \cdot (\mathbf{k} + \mathbf{k}')}. \end{aligned} \quad (5)$$

* miru.lee@uni-goettingen.de

† matthias.krueger@uni-goettingen.de

The homogeneity thus entails $\mathbf{k} = -\mathbf{k}'$, i.e.,

$$G(\mathbf{k}, \mathbf{k}', \omega) = (2\pi)^3 G(\mathbf{k}, \omega) \delta(\mathbf{k} + \mathbf{k}'). \quad (6)$$

Or,

$$G(\mathbf{k}_{\parallel}, z, \mathbf{k}'_{\parallel}, z', \omega) = (2\pi)^2 G(\mathbf{k}_{\parallel}, z - z', \omega) \delta(\mathbf{k}_{\parallel} + \mathbf{k}'_{\parallel}). \quad (7)$$

Plugging it into Eq. (4), one arrives at

$$\Gamma = \frac{\kappa^2 n_A^2 l^4 \pi^2}{\omega} \text{Im} \left\{ \int_{-\infty}^{\infty} \frac{d^2 \mathbf{k}_{\parallel}}{(2\pi)^2} G(\mathbf{k}_{\parallel}, 0, \omega) e^{-\frac{1}{2} k_{\parallel}^2 l^2} \right\}, \quad (8)$$

which we use to evaluate the damping coefficient both numerically and analytically.

BOUNDARY CONDITIONS

Regarding the geometry of the system, it has the surface at $z = 0$ in the xy plane, while extending infinitely in the x and y directions. For $z > 0$, it is a vacuum, i.e., no phonon can exist. The boundary conditions (BC) at $z = 0$ are given by [11–14]

$$\sigma_{xz}(\mathbf{r}_{\parallel}, \omega) = \kappa X(\omega) e^{-\frac{r_{\parallel}^2}{l^2}}, \quad (9)$$

while other components are zero. Here, $\boldsymbol{\sigma}(\mathbf{r}, \omega)$ is the Cauchy stress tensor, which is defined as

$$\boldsymbol{\sigma} = \rho(c_L^2 - 2c_T^2) \nabla \cdot \mathbf{u} + \rho c_T^2 (\nabla \mathbf{u} + (\nabla \mathbf{u})^T). \quad (10)$$

Note that the BC on the surface suggest that the displacement field $u_x(\mathbf{r}, \omega)$ is linearly proportional to the position of the probe $X(\omega)$, containing the phase information with respect to $X(\omega)$, which, in turn, yields a finite damping coefficient.

For $-d < z \leq 0$, we have the first layer (the coating) of the solid whose properties are characterized by $c_{L0}(\omega)$, $c_{T0}(\omega)$, and ρ_0 . The second layer (the substrate) expands for $-\infty < z < -d$ with $c_{L1}(\omega)$, $c_{T1}(\omega)$, and ρ_1 . The BC at $z = -d$ require that the displacement field and traction are continuous [15],

$$\begin{aligned} \lim_{z \rightarrow -d^+} \mathbf{u}(\mathbf{r}, \omega) &= \lim_{z \rightarrow -d^-} \mathbf{u}(\mathbf{r}, \omega), \\ \lim_{z \rightarrow -d^+} \hat{\mathbf{e}}_z \cdot \boldsymbol{\sigma}(\mathbf{r}, \omega) &= \lim_{z \rightarrow -d^-} \hat{\mathbf{e}}_z \cdot \boldsymbol{\sigma}(\mathbf{r}, \omega), \end{aligned} \quad (11)$$

where $\hat{\mathbf{e}}_z$ is the unit vector in the z direction. The Dirichlet and Neumann BC in the main text are the special cases of the above BC.

TRAVELING VS. EVANESCENT WAVE

Here, we show that traveling waves yield the elastic contribution, and evanescent waves the viscous contribution. Since any wave can be expressed by a superposition of plane waves, an ansatz of the transverse motion of the solid ([Eq. (2)] in the main text) can be written as

$$G_T(\mathbf{k}_{\parallel}, z - z', d, \omega) = C_0(\mathbf{k}_{\parallel}, d, \omega) e^{q_T(z - z')} + C_1(\mathbf{k}_{\parallel}, d, \omega) e^{-q_T(z - z')}, \quad (12)$$

where $q_T = (k_{\parallel}^2 - \omega^2/c_T^2)^{1/2}$, and $C_0(\mathbf{k}_{\parallel}, d, \omega)$ ($C_1(\mathbf{k}_{\parallel}, d, \omega)$) is an amplitude of outgoing (incoming) wave. The longitudinal counterpart can be similarly written with $q_L = (k_{\parallel}^2 - \omega^2/c_L^2)^{1/2}$, which then gives us the full solution $G = G_T + G_L$. From the ansatz, it follows that if $k_{\parallel} \leq \omega/c_T$, the solution represents a traveling wave in the z direction. Contrarily, if $k_{\parallel} \geq \omega/c_T$, then it decays exponentially in the z coordinate, i.e., an evanescent wave.

Notice also that the integral in Eq. (8) runs in \mathbf{k}_{\parallel} space, along which there may exist branches or singularities. Consequently, the integral can be divided into many parts according to the branch or/and singular points,

$$\begin{aligned} \Gamma &= \frac{\kappa^2 n_A^2 l^4}{4\omega} \text{Im} \left\{ \int_0^{2\pi} d\theta \left[\int_0^{k_{s,1}} dk_{\parallel} k_{\parallel} G(\mathbf{k}_{\parallel}, 0, d, \omega) e^{-\frac{1}{2} k_{\parallel}^2 l^2} + \int_{k_{s,1}}^{k_{s,2}} dk_{\parallel} k_{\parallel} G(\mathbf{k}_{\parallel}, 0, d, \omega) e^{-\frac{1}{2} k_{\parallel}^2 l^2} \right. \right. \\ &\quad \left. \left. + \int_{k_{s,2}}^{k_{s,3}} dk_{\parallel} k_{\parallel} G(\mathbf{k}_{\parallel}, 0, d, \omega) e^{-\frac{1}{2} k_{\parallel}^2 l^2} + \dots + \int_{k_{s,N}}^{\infty} dk_{\parallel} k_{\parallel} G(\mathbf{k}_{\parallel}, 0, d, \omega) e^{-\frac{1}{2} k_{\parallel}^2 l^2} \right] \right\} \end{aligned} \quad (13)$$

where $k_{s,n}$ $n \in \{1, 2, \dots, N\}$ are the branch and singular points of the Green's function. In what follows, we show that the terms running up to $k_{s,N}$ integrate traveling waves resulting in the elastic contribution, and the last term evanescent waves resulting in the viscous contribution.

Let us exemplarily consider the transverse mode. The Green's function at $z = z'$ (the argument is henceforth omitted) at the limit of $d \gg \lambda$ reads,

$$G_{\text{T}}(\mathbf{k}_{\parallel}, \omega) = \frac{\sin^2 \theta}{\rho_0 c_{\text{T}0}^2 q_{\text{T}0}}. \quad (14)$$

The branch point is located at $k_s = \omega/c_{\text{T}0}$. Note that this branch point coincides with the singularity. The integration is thus divided into two parts. The first part integrates traveling waves,

$$\frac{\kappa^2 n_{\text{A}}^2 l^4}{4\omega} \int_0^{2\pi} d\theta \int_0^{\omega/c_{\text{T}0}} dk_{\parallel} k_{\parallel} \frac{\sin^2 \theta}{\rho_0 c_{\text{T}0}^2 q_{\text{T}0}} e^{-\frac{1}{2} k_{\parallel}^2 l^2} = -\frac{\pi^{3/2} \kappa^2 n_{\text{A}}^2 l^3 e^{-l^2 \omega^2 / (2c_{\text{T}0}^2)}}{2^{5/2} c_{\text{T}0}^2 \rho_0 \omega} \operatorname{erf}\left(\frac{-il\omega}{\sqrt{2}c_{\text{T}0}}\right), \quad (15)$$

where $\operatorname{erf}(x)$ is the error function. Expanding it at small ω and taking the imaginary part, one arrives at

$$\operatorname{Im} \left\{ -\frac{\pi^{3/2} \kappa^2 n_{\text{A}}^2 l^3 e^{-l^2 \omega^2 / (2c_{\text{T}0}^2)}}{2^{5/2} c_{\text{T}0}^2 \rho_0 \omega} \operatorname{erf}\left(\frac{-il\omega}{\sqrt{2}c_{\text{T}0}}\right) \right\} = \frac{\pi \kappa^2 n_{\text{A}}^2 l^4}{4} \sqrt{\frac{\rho_0}{\mu_0^3}} + \mathcal{O}\left(\frac{1}{Q^2}, \frac{l^2}{\lambda^2}\right). \quad (16)$$

Note that the leading order of this contribution is *independent* of viscosity η_0 .

The second part, on the contrary, takes care of the evanescent wave solution

$$\frac{\kappa^2 n_{\text{A}}^2 l^4}{4\omega} \int_0^{2\pi} d\theta \int_{\omega/c_{\text{T}0}}^{\infty} dk_{\parallel} k_{\parallel} \frac{\sin^2 \theta}{\rho_0 c_{\text{T}0}^2 q_{\text{T}0}} = \frac{\pi^{3/2} \kappa^2 n_{\text{A}}^2 l^3 e^{-l^2 \omega^2 / (2c_{\text{T}0}^2)}}{2^{5/2} c_{\text{T}0}^2 \rho_0 \omega}. \quad (17)$$

Repeating the same procedure leads us to

$$\operatorname{Im} \left\{ \frac{\pi^{3/2} \kappa^2 n_{\text{A}}^2 l^3 e^{-l^2 \omega^2 / (2c_{\text{T}0}^2)}}{2^{3/2} c_{\text{T}0}^2 \rho_0 \omega} \right\} = \frac{\pi^{5/2} \kappa^2 n_{\text{A}}^2 l^3 \eta_0}{2^{5/2} \mu_0^2} + \mathcal{O}\left(\frac{1}{Q^2}, \frac{l^2}{\lambda^2}\right). \quad (18)$$

Unlike the elastic contribution from traveling waves, the leading order is linearly proportional to the viscosity η_0 . Putting them together, we find

$$\begin{aligned} \Gamma_{\text{T}}^{\infty} &= \frac{\pi \kappa^2 n_{\text{A}}^2 l^4}{4} \sqrt{\frac{\rho_0}{\mu_0^3}} + \frac{\pi^{3/2} \kappa^2 n_{\text{A}}^2 l^3 \eta_0}{2^{5/2} \mu_0^2} + \mathcal{O}\left(\frac{1}{Q^2}, \frac{l^2}{\lambda^2}\right) \\ &= \frac{\pi \kappa^2 n_{\text{A}}^2 l^4}{4\rho_0 c_{\text{T}0}^3} \left(1 + \sqrt{\frac{\pi}{2}} \frac{\eta_0}{\rho_0 c_{\text{T}0} l}\right) + \mathcal{O}\left(\frac{1}{Q^2}, \frac{l^2}{\lambda^2}\right). \end{aligned} \quad (19)$$

It is noteworthy that the existence of a branch point or a singularity at a finite value of k_{\parallel} directly indicates the existence of a traveling wave. If the Green's function exhibits no such point, then the corresponding wave is purely evanescent.

FUNDAMENTAL SOLUTIONS

For the Dirichlet BC, the Green's function at the surface ($z = z' = 0$), for d being the smallest length scale, is given by

$$G(\mathbf{k}_{\parallel}, d, \omega) = \frac{d}{c_{\text{T}0}^2 \rho_0} + \mathcal{O}(d^3). \quad (20)$$

The leading order has no branch or singular point, meaning that it is evanescent. Since it is constant in \mathbf{k}_{\parallel} space, the above expression becomes a delta function in \mathbf{r}_{\parallel} space,

$$G(\mathbf{r}_{\parallel} - \mathbf{r}'_{\parallel}, d, \omega) = \frac{d}{c_{\text{T}0}^2 \rho_0} \delta^{(2)}(\mathbf{r}_{\parallel} - \mathbf{r}'_{\parallel}) + \mathcal{O}(d^3). \quad (21)$$

For the Neumann BC, the Green's function reads

$$G(\mathbf{k}_{\parallel}, d, \omega) = \frac{c_{\text{L0}}^2 (k_{\parallel}^2 - q_{\text{L0}}^2) (k_y^2 + q_{\text{T0}}^2) - 2c_{\text{T0}}^2 k_y^2 (k_{\parallel}^2 - 2q_{\text{L0}}^2 + q_{\text{T0}}^2)}{dc_{\text{T0}}^2 \rho_0 q_{\text{T0}}^2 (c_{\text{L0}}^2 (k_{\parallel}^2 - q_{\text{L0}}^2) (k_{\parallel}^2 + q_{\text{T0}}^2) - 2c_{\text{T0}}^2 k_{\parallel}^2 (k_{\parallel}^2 - 2q_{\text{L0}}^2 + q_{\text{T0}}^2))} + \mathcal{O}(d). \quad (22)$$

One can easily tell it can be either a traveling or evanescent wave due to the existence of the singular point. By finding the real space counterpart, one can easily identify the dimensional nature of the solution. Assuming $c_{\text{T0}} = \sqrt{3}c_{\text{L0}}$, it is

$$G(\mathbf{r}_{\parallel} - \mathbf{r}'_{\parallel}, d, \omega) = \frac{8(y - y')^2 K_0 \left(-\frac{i|\mathbf{r}_{\parallel} - \mathbf{r}'_{\parallel}| \omega}{c_{\text{T0}}} \right) + 3(x - x')^2 K_0 \left(-\frac{i\sqrt{3}|\mathbf{r}_{\parallel} - \mathbf{r}'_{\parallel}| \omega}{2\sqrt{2}c_{\text{T0}}} \right)}{16\pi\rho_0 c_{\text{T0}}^2 |\mathbf{r}_{\parallel} - \mathbf{r}'_{\parallel}|^2 d} + \mathcal{O}(d), \quad (23)$$

where K_0 is the Bessel function of the second kind of the zeroth order, a form of surface (2D) waves.

At a large $d \gg \lambda$ on the other hand, the Green's function is given by

$$G(\mathbf{k}_{\parallel}, \omega) = \frac{c_{\text{L0}}^2 (k_{\parallel}^2 - q_{\text{L0}}^2) (k_y^2 + q_{\text{T0}}^2) - 2c_{\text{T0}}^2 k_y^2 (k_{\parallel}^2 - 2q_{\text{L0}}q_{\text{T0}} + q_{\text{T0}}^2)}{c_{\text{T0}}^2 \rho_0 q_{\text{T0}}^2 (c_{\text{L0}}^2 (k_{\parallel}^2 - q_{\text{L0}}^2) (k_{\parallel}^2 + q_{\text{T0}}^2) - 2c_{\text{T0}}^2 k_{\parallel}^2 (k_{\parallel}^2 - 2q_{\text{L0}}q_{\text{T0}} + q_{\text{T0}}^2))}. \quad (24)$$

This, again, can be either a traveling or evanescent wave, however, finding the exact expression of the real space counterpart seems difficult. A simpler way to see the dimensionality of the fundamental solution is to only consider the transverse mode, i.e., Eq. (14). In real space, it is given by

$$G_{\text{T}}(\mathbf{r}_{\parallel} - \mathbf{r}'_{\parallel}, \omega) = -\frac{(y - y')^2 e^{\frac{i|\mathbf{r}_{\parallel} - \mathbf{r}'_{\parallel}| \omega}{c_{\text{T0}}}}}{2\pi\rho_0 c_{\text{T0}}^2 |\mathbf{r}_{\parallel} - \mathbf{r}'_{\parallel}|^3}, \quad (25)$$

which is a spherical (3D) wave solution.

Upon arriving at these fundamental wave solutions, no assumption on $\tilde{\eta}$ is made. In fact, $\tilde{\eta}$ can only be defined after obtaining Eq. (24). This means, mathematically, that [Eqs. (7) and (8)] in the main text are valid for all $\tilde{\eta}$.

THE DAMPING COEFFICIENT FOR AN ARBITRARY INTERACTION AT THE LIMITING CASES

Let us consider a general way to formulate the probe-sample interaction F . Such an interaction arises from the underlying pairwise probe-atom interaction $g(\mathbf{X}, \mathbf{r}_{\parallel}, \omega)$ (it can easily be generalized for vectors as well),

$$F(X, \omega) = n_{\text{A}} \int_{-\infty}^{\infty} d^2\mathbf{r}_{\parallel} g(X, \mathbf{r}_{\parallel}, \omega). \quad (26)$$

Expanding the pairwise interaction in u_x , one finds

$$g(X, \mathbf{r}_{\parallel}, \omega) = g(X, \mathbf{r}_{\parallel}) + \frac{\partial}{\partial x} g(X, \mathbf{r}_{\parallel}) \cdot u_x(\mathbf{r}_{\parallel}, \omega) + \dots \quad (27)$$

If $\sqrt{\langle u_x^2(\mathbf{r}_{\parallel}, \omega) \rangle} \ll |\mathbf{r}_{\parallel} - X|$ is assumed, the first term can be seen as the pairwise interaction in phase with the motion of X , and the second term out of phase. Now one can calculate the damping coefficient similarly as Eq. (2).

Let us consider the case of small d . For the Dirichlet BC, we use Eq. (20) for the Green's function and perform the integral. Because the Green's function is independent of \mathbf{k}_{\parallel} for the leading order of d , the damping coefficient is given simply by the integration of the interaction,

$$\Gamma = \frac{n_{\text{A}}^2 \eta_0 d}{\mu_0^2} \int_{-\infty}^{\infty} \frac{d^2\mathbf{k}_{\parallel}}{(2\pi)^2} \left| \frac{\partial}{\partial x} g(X, \mathbf{k}_{\parallel}) \right|^2. \quad (28)$$

The linear dependence of the damping coefficient on the coating thickness d is thus universal to any type of interaction.

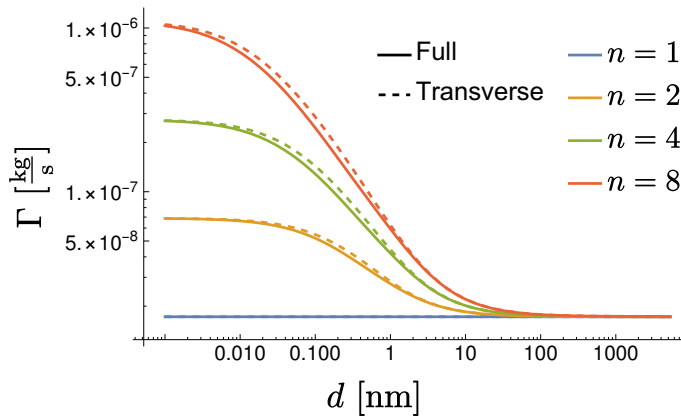


FIG. 1. Comparison between the full (transverse and longitudinal) and transverse solution calculations. Γ 's obtained from the transverse solution are scaled by the factor in Eq. (32).

For the Neumann BC, the Green's function is given by Eq. (22), which, for $c_{T0} = \sqrt{3}c_{L0}$, reduces to

$$G'(k_{\parallel}, \omega) = \int_0^{2\pi} d\theta G(\mathbf{k}_{\parallel}, \omega) = \frac{\pi(11c_{T0}^2 k_{\parallel}^2 - 6\omega^2)}{d\rho_0(c_{T0}^2 k_{\parallel}^2 - \omega^2)(8c_{T0}^2 k_{\parallel}^2 - 3\omega^2)}. \quad (29)$$

Note that $g(X, \mathbf{k}_{\parallel})$ is azimuthally symmetric, so that it can be factored out of the integral over θ . The integral over k_{\parallel} can be done by means of the residue theorem due to the singularities at

$$k_{\parallel} = \frac{\omega}{c_{T0}(\omega)}, \quad k_{\parallel} = \sqrt{\frac{3}{8}} \frac{\omega}{c_{T0}(\omega)}, \quad (30)$$

yielding the elastic contribution from traveling waves. The remaining integrals that are associated with the residue theorem contributes to higher order terms in ω (i.e., $\mathcal{O}(d/\lambda)$, see Ref. [4] for the detailed calculation).

The resulting damping coefficient for the leading order of ω and d is

$$\Gamma = \frac{11}{64\mu_0|\omega|d} \langle F(X) \rangle^2. \quad (31)$$

The above expression is universal to any types of interaction for the leading order of ω . In fact, the elastic contribution is agnostic to the form of interaction, the characteristic of which we named *universality* in Ref. [4]. To see this, let us consider the locations of the singularities at $\omega \rightarrow 0$; the singularities are approaching to $k_{\parallel} = 0$ as $\omega \rightarrow 0$. This means the Green's function behaves like a delta function, and therefore the interaction has to be evaluated at $k_{\parallel} = 0$. By Eq. (26), $g(X, \mathbf{k}_{\parallel} = \mathbf{0}) = F(X)$ can be found; the damping coefficient does not depend on the form of the interaction. For detailed discussions and derivations of the universality of the elastic contribution, we refer the readers to Ref. [4].

TRANSVERSE VS. FULL SOLUTIONS

In the main text, the cases for arbitrary n are calculated with only the transverse waves considered. In Fig. 1, we present, for a few selected n values, a comparison between the full (transverse and longitudinal) and the transverse wave solutions. Note that in the plot, the damping coefficients calculated from the transverse solution are scaled by a factor

$$\frac{\Gamma^{\infty}}{\Gamma_{\text{T}}^{\infty}} = \frac{6.88\sqrt{2}}{\pi\sqrt{\pi}}, \quad (32)$$

which is nothing but the ratio of [Eq. (6)] in the main text to the viscous contribution in Eq. (19). From Fig. 1, it is clear that the transverse waves can capture the essential physics when it comes to the friction calculation.

FINDING THE PEAKS

For $\tilde{\eta} \ll 1$, the damping coefficient Γ exhibits peaks at $d \approx \lambda$, resulting from resonances of the excited waves. We identify that there are two types of resonances: body waves and surface waves. The former is due to interference of outgoing and reflected waves. The surface wave resonance, on the other hand, is related to the singularity of the Green's function in Fourier space $(\mathbf{k}_{\parallel}, \omega)$ [16–18].

Let us begin with the peak of the surface wave. From Eq. (24), one finds that the position of singularity is at

$$k_s(\omega) = \frac{\sqrt{3 + \sqrt{3}}}{2} \frac{\omega}{c_{T0}(\omega)}. \quad (33)$$

The peak position of surface wave is thus

$$d^{\text{surface}}(\omega) = \frac{1}{2} \text{Re} \left\{ \frac{2\pi}{k_s(\omega)} \right\}. \quad (34)$$

The peaks of body waves can be found by considering the plane waves, i.e., evaluating the Green's function at $\mathbf{k}_{\parallel} = \mathbf{0}$,

$$G(\mathbf{0}, d, \omega) = \begin{cases} \frac{1}{\rho_0 c_{T0}} \tan\left(\frac{d\omega}{c_{T0}}\right) & n = 0 \\ -\frac{1}{\rho_0 c_{T0}} \cot\left(\frac{d\omega}{c_{T0}}\right) & n \rightarrow \infty, \end{cases} \quad (35)$$

from which the peak positions are obtained,

$$d_m^{\text{body}}(\omega) = \begin{cases} \frac{\pi c'_{T0}}{\omega} \left(\frac{1}{2} + m\right) & n = 0 \\ \frac{\pi c_{T0}}{\omega} (1 + m) & n \rightarrow \infty, \end{cases} \quad m \in \{0, 1, 2, \dots\} \quad (36)$$

Figures 2 (a) and (b) show the peak positions for $n = 0$ and $n \rightarrow \infty$, respectively. The detected peak positions agree with our predictions as shown in the subsequent plots. Note that in Fig. 2 (b) we do not observe the plateau from the viscous contribution before the peaks. This is because $\tilde{\eta}$ and Q are inversely related to each other, resulting in $lQ \approx \lambda$; the peaks occur before the first plateau of the viscous contribution fully establishes.

DEFINING THE REGIMES IN [FIG. 5] IN THE MAIN TEXT

The scaling behavior of Γ can be understood by studying $\lim_{d \rightarrow 0} \Gamma$ and Γ^{∞} ,

$$\frac{\lim_{d \rightarrow 0} \Gamma}{\Gamma^{\infty}} = \frac{n^3 \zeta^{\text{ela}} + n^2 \zeta^{\text{vis}} \tilde{\eta}}{\zeta^{\text{ela}} + \zeta^{\text{vis}} \tilde{\eta}}. \quad (37)$$

Keep in mind that $\zeta^{\text{ela}}/\zeta^{\text{vis}} \approx 1$. The numerator is the damping coefficient of the substrate and the denominator that of the coating. To begin with, let us consider the numerator, from which a separating line

$$n = \tilde{\eta} \quad (38)$$

can be defined. If $n \gg \tilde{\eta}$, the elastic contribution of the substrate is much larger than the viscous contribution of the substrate.

Another line can be found when comparing the elastic contribution of the substrate with the viscous contribution of the coating,

$$n = \sqrt[3]{\tilde{\eta}}. \quad (39)$$

If $\sqrt[3]{\tilde{\eta}} \lesssim n \lesssim \tilde{\eta}$, one finds $\zeta^{\text{vis}} \tilde{\eta} \lesssim \zeta^{\text{ela}} n^3$; the viscous contribution of the coating is smaller than the elastic contribution of the substrate. Because the latter decays at a slow rate $d \approx Ql$, it is visible as shown in [Fig. 3] for $n = 100$ in the main text. Another case is when $\sqrt[3]{\tilde{\eta}} \lesssim n \lesssim 1$. The elastic contribution of the substrate is larger than the viscous contribution of the coating. In this case, the damping coefficient remains constant until $d \approx \lambda$.

Comparing the viscous contribution of the substrate to the elastic contribution of the coating defines yet another line,

$$n = \sqrt{\tilde{\eta}^{-1}}. \quad (40)$$

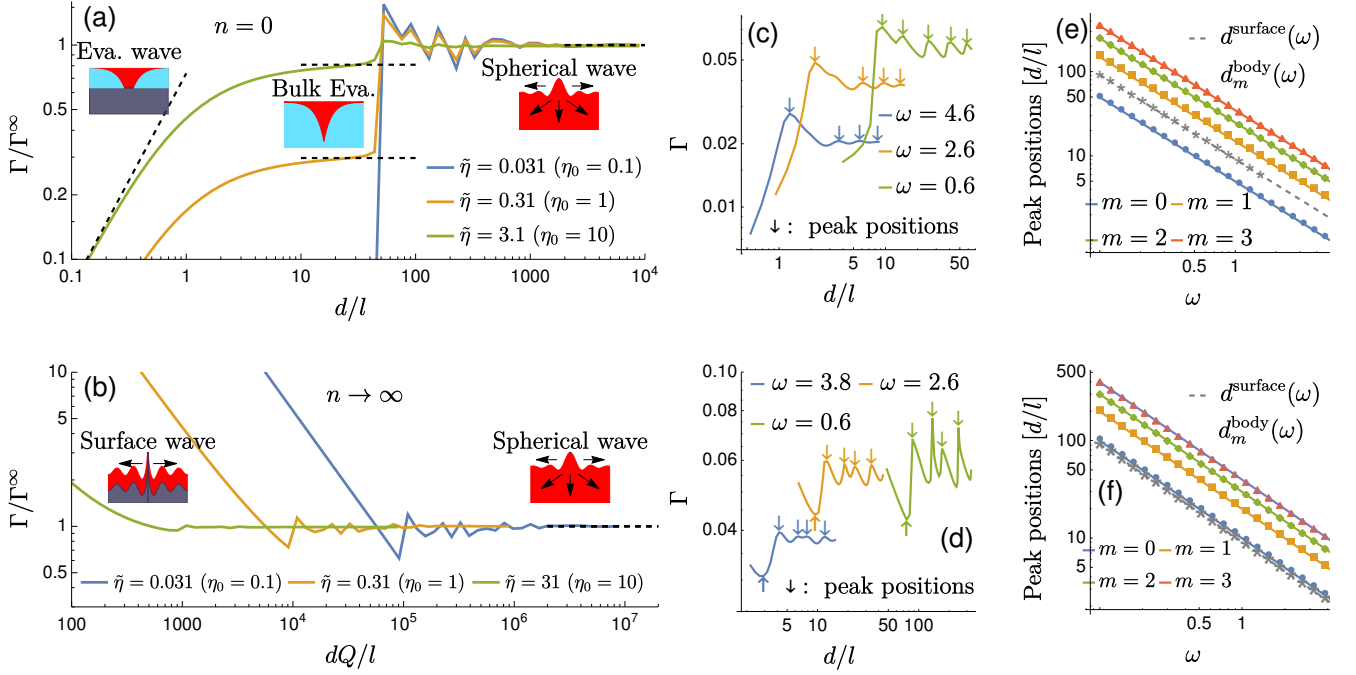


FIG. 2. (a) and (b): The damping coefficient Γ as a function of the depth of the first layer d for $n = 0$ (a) and $n \rightarrow \infty$ (b). The solid lines are numerical evaluations of the friction, whereas the black dashed lines are the asymptotes. The parameters are $\kappa = 1$, $l = 1$, $\omega = 0.1$, $n_A = 1$, $\rho = 1$, and $\mu = 10$, resulting in $\lambda/l \approx 200$. (c) and (d): A closer look of the damping coefficient near the peak positions with different values of ω at $\tilde{\eta} = 0.31$. (e) and (f): The first few peak positions as a function of ω at $\tilde{\eta} = 0.31$. The points are the detected peak positions from the numerical evaluations, and the lines are the exact peak positions.

A case of interest would be $1 \lesssim \tilde{\eta} \lesssim n^{-2}$, where the viscous contribution of the substrate is much larger than the elastic contribution of the coating. This should result in two plateaus, one from the viscous contribution of the coating at $d \approx Ql$, the other from the elastic contribution at $d \approx \lambda$ similar to those seen in Fig. 2 (a). However, this regime is inaccessible since Q becomes inevitably large for small $\tilde{\eta}$ so that Ql becomes comparable to or larger than λ as discussed above. The line defined by Eq. (40) is thus not shown in [Fig. 5] in the main text.

GENERALIZING [EQ. (9)] IN THE MAIN TEXT

Even if the assumptions of n being real and $\rho_0 = \rho_1$ are relaxed, one can still gain useful insights into the scaling behavior of friction by constructing an equation similar to [Eq. (9)] in the main text (or Eq. (37) here in SM). This can be done by finding and comparing the bulk damping coefficients of the substrate and the coating from [Eq. (3)] in the main text,

$$\frac{\lim_{d \rightarrow 0} \Gamma}{\Gamma^\infty} = n'^3 \frac{\rho_0}{\rho_1} \left(\frac{\zeta^{\text{ela}} + n' \zeta^{\text{vis}} \frac{\eta_1}{c'_{T0} \rho_1 l}}{\zeta^{\text{ela}} + \zeta^{\text{vis}} \frac{\eta_0}{c'_{T0} \rho_0 l}} \right) \quad (41)$$

with $\text{Re}\{n\} = n' + \mathcal{O}(\omega^3) = c'_{T0}/c'_{T1} + \mathcal{O}(\omega^3)$.

-
- [1] R. Kubo, M. Toda, and N. Hashitsume, *Statistical physics II: nonequilibrium statistical mechanics*, Vol. 31 (Springer Science & Business Media, Berlin, 2012).
[2] R. Zwanzig, *Nonequilibrium statistical mechanics* (Oxford University Press, Oxford, 2001).
[3] M. Krüger and C. Maes, *Journal of Physics: Condensed Matter* **29**, 064004 (2016).
[4] M. Lee, R. L. Vink, C. A. Volkert, and M. Krüger, *Physical Review B* **104**, 174309 (2021).
[5] W. Eckhardt, *Physical Review A* **29**, 1991 (1984).

- [6] M. Krüger, T. Emig, and M. Kardar, *Physical Review Letters* **106**, 210404 (2011).
- [7] M. Krüger, G. Bimonte, T. Emig, and M. Kardar, *Physical Review B* **86**, 115423 (2012).
- [8] E. M. Lifshitz and L. P. Pitaevskii, *Statistical physics: theory of the condensed state*, Vol. 9 (Elsevier, Oxford, 2013).
- [9] G. Agarwal, *Physical Review A* **11**, 230 (1975).
- [10] C. M. Van Vliet, *Equilibrium And Non-equilibrium Statistical Mechanics (New And Revised Printing)* (World Scientific Publishing Company, 2008).
- [11] L. Landau, E. Lifshitz, J. Sykes, and W. Reid, *Theory of elasticity: Volume 7 of course of theoretical physics*, Vol. 7 (Elsevier, Oxford, 1986).
- [12] W. N. Findley, J. S. Lai, and K. Onaran, *Creep and Relaxation of Nonlinear Viscoelastic Materials, with an Introduction to Linear Viscoelasticity* (North-Holland Publishing Company, New York, N.Y., 2013).
- [13] E. Lee, *Quarterly of Applied Mathematics* **13**, 183 (1955).
- [14] R. D. Mindlin, *physics* **7**, 195 (1936).
- [15] L. M. Brekhovskikh, *Waves in layered media* (Academic Press, New York, 1980).
- [16] B. Persson and R. Ryberg, *Physical Review B* **32**, 3586 (1985).
- [17] A. Volokitin, B. Persson, and H. Ueba, *Physical Review B* **73**, 165423 (2006).
- [18] B. Persson, E. Tosatti, D. Fuhrmann, G. Witte, and C. Wöll, *Physical Review B* **59**, 11777 (1999).